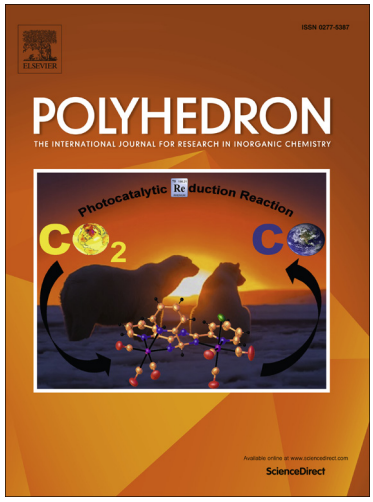

Porous nickel oxide pseudo-capacitive materials fabricated by Ni-Schiff base nanostructures template

Kuaibing Wang, Bing Jin, Aimin Lu, Xuefei Luo, Ying Shi

PII: S0277-5387(16)30211-X
DOI: http://dx.doi.org/10.1016/j.poly.2016.05.058
Reference: POLY 12032

To appear in: *Polyhedron*

Received Date: 29 March 2016
Accepted Date: 29 May 2016

Please cite this article as: K. Wang, B. Jin, A. Lu, X. Luo, Y. Shi, Porous nickel oxide pseudo-capacitive materials fabricated by Ni-Schiff base nanostructures template, *Polyhedron* (2016), doi: http://dx.doi.org/10.1016/j.poly.2016.05.058

Porous nickel oxide pseudo-capacitive materials fabricated by Ni-Schiff base nanostructures template

Kuaibing Wang,[a,b]* Bing Jin,[a] Aimin Lu,[a] Xuefei Luo,[a] and Ying Shi[a]

[a]Department of Chemistry, College of Science, Nanjing Agricultural University, Nanjing 210095, P. R. China

[b]State Key Laboratory of Coordination Chemistry, Nanjing University, Nanjing 210093, P. R. China

E-mail: wangkb@njau.edu.cn; Tel/Fax: +86-025-84396697

ABSTRACT: Three nanoscale Ni-Schiff-base coordination polymer particles have been firstly prepared in poor solvent (DMF) through a precipitation method. XRD, TGA and EA results show that as-synthesized compounds are either amorphous or crystalline. High temperature annealing of these Ni-based compounds can result in pseudo-capacitive NiO electrodes. Series of electrochemical measurements illustrated that the as-prepared NiO material, especially for NiO nanospheres could deliver a maximum specific capacitance of 153 F g^{-1} and good stability over 1000 cycles with the capacitance retention of 100%, indicating the morphology and resistance effect on the diffusion-controlled redox reaction between the OH^- ions and the NiO samples.

Keywords: Coordination polymer particles; Nickel oxide; Pseudo-capacitance; Schiff base; Energy storage.

1. Introduction

Nanoscale coordination polymer particles (NCPPs), including include crystalline and amorphous state, have recently gained immense attention as hybrid materials due to their promising applications in various fields including drug delivery, ion exchange, gas storage, and magnetic resonance imaging [1-6]. NCPPs can be successfully tuned with tailorable morphologies and physicochemical properties by careful selection of both metal ions and organic ligands. Introduction of functional groups such as pyridine, amide, and aromatic rings onto the organic building blocks, which can provide many coordinate sites and are capable of forming diversified weak interactions like hydrogen bonding or π–π stacking, have been found to promote the requisite cross-linking network [7]. In this regard, various NCPPs with distinct morphologies and porosity would be fabricated by designing the chelating ligands, and consequently influencing the resulting chemo-, physic- and bio-properties.

To date, advances have been made in the miniaturization of coordination polymer materials to the micro- and nanometer scale [8-12]. Among these materials, an alternative and effective strategy, which is based on infinite coordination polymerization followed by precipitation with a poor solvent, has been reported and frequently used. This approach has so far been usually exploited to prepare fluorescent metal-organic microspheres and other shapes by reactions of organic linkers with zinc or cupric salts [13-16]. Following this strategy, the wide-ranging NCPPs are demonstrated for several types of functional species, such as magnetic nanoparticles, core-shell structures, and luminescent quantum dots (QDs) and so forth [13,17,18].

Using as a kind of soft template to synthesize inorganic compounds extend the utilization range of NCPPs and has even been proven very effective in the synthesis of a wide variety of hollow or porous particles [19-21]. Template methods possess major advantages in control over the size and shape of the products. Besides, in comparison with hard template, NCPPs do not need tedious synthetic procedures and harsh removal process. Moreover, lots of released gases generated in annealing process can form various inorganic compounds or hybrids with porous or hollow architecture. In this manuscript, scarce Ni-based NCPPs have been fabricated by the reactions of the newly-synthesized Schiff-base ligands with Ni ions and characterized by XRD, TGA, EA and IR. To examine the template function of Ni-based NCPPs, NiO electrode materials have also been prepared and investigated by series of electrochemical measurements.

2. Experimental

2.1 Synthesis of Schiff base ligand and Ni-based CPPs

The Schiff-base ligand, 3,5-bis-((pyridin-3-ylmethylene)amino) benzoic acid (**L_1**), 4-((pyridin-3-ylmethylene)amino)benzoic acid (**L_2**) and 4-((pyridin-4-ylmethylene)amino)benzoic acid (**L_3**), was synthesized by reacting the corresponding amino-containing benzoic acid with nicotinaldehyde through aldehyde-ammonia condensation reaction (details see Fig. S1-S3). ESI-MS for **L_1**: m/z 329.17 $[M-H]^-$; **L_2**: m/z 225.07 $[M-H]^-$; **L_3**: m/z 225.07 $[M-H]^-$. Elem. Anal. for **L_1**: C, 69.10; H, 4.32; N, 17.01%. **L_2**: C, 69.21; H, 4.53; N, 12.36%. **L_3**: C, 68.97; H,

4.48; N, 12.39%.

For synthesis of Ni-based CPPs, a Schiff-base ligand (1.5 mmol) was introduced into a flask containing *N,N*-dimethylformamide solvent (30 mL), and the flask was heated up to 70 ℃ to form a clear solution. Then 1.5 mL of $Ni(OAc)_2$ (0.5 M) aqueous solution was added into the clear solution drop by drop under vigorous stirring, and a green precipitate occurred slowly. After stirring for 60 min, the precipitate was collected by centrifugation, and washed several times with ethanol via continuous centrifugation and re-dispersion cycles. Notably, for convenient discussion, the as-synthesized CPPs were denoted as CPP-1, CPP-2 and CPP-3 corresponding to the ligand $\mathbf{L_1}$, $\mathbf{L_2}$ and $\mathbf{L_3}$, respectively. IR for CPP-1 (KBr pellet, cm^{-1}): 1610 (s), 1532 (s), 1408 (s), 1320 (w), 1186 (m), 1093 (m), 950 (w), 866 (w), 793 (w), 692 (m), 649 (w). For CPP-2: 1607 (s), 1537 (s), 1392 (s), 1248 (w), 1196 (m), 1082 (m), 1031 (m), 855 (m), 793 (m), 679 (m), 597 (w). For CPP-3: 1599 (s), 1537 (s), 1382 (s), 1237 (w), 1175 (m), 1093 (w), 1041 (w), 938 (w), 793 (s), 680 (s), 546 (m). Elem. Anal. for CPP-1: C, 50.51; H, 4.77; N, 12.96%. CPP-2: C, 55.94; H, 4.47; N, 10.99%. CPP-3: C, 46.52; H, 4.41; N, 8.17%.

2.2 Synthesis of NiO nanostructures with different shapes

For synthesis of NiO nanostructures, the as-synthesized coordination polymers of CPP-1–CPP-3 were separately ground, dispersed in ethanol and dried in 35 ℃ for 4 h in a corundum crucible. Then these precursors were heated in air to 450 ℃ and maintained for 1 hour, and allowed to cool down to room temperature spontaneously.

As a result, NiO with different shapes were obtained by re-dispersion with ethanol, centrifugation, and dried under vacuum, respectively.

2.3 Electrode preparation

The working electrodes were prepared as follows. The mixture containing 80 wt.% NiO, 15 wt.% acetylene black and 5 wt.% polytetrafluoroethylene (PTFE) was well mixed, and then was incorporated in nickel foam (1 cm × 1 cm), and the typical mass load of electrode materials ranged in 4.8–7.4 mg after pressed by Manual Rolling Press. Furthermore, these electrodes were separately soaked into 6.0 M KOH solution overnight before the electrochemical test.

2.4 Methods and Measurements

Solvents and all other chemicals were obtained from commercial sources and used as received unless otherwise noted; water used throughout all experiment was purified with the Millipore system (18.2 MΩ cm). X-ray powder diffraction (XRD) data were collected on a Bruker D8 Advance instrument using Cu_K radiation (= 1.54056 A°) at room temperature. Fourier-transformed infrared (FT-IR) spectra were obtained on a Bruker Vector 22 FT-IR spectrophotometer using KBr pellets. Elemental analyses of C, H, and N were performed on an Elementar Vario MICRO Elemental Analyzer at the Analysis Centre of Nanjing University. Thermo-gravimetrical analyses (TGA) were performed in a N_2 atmosphere (a flow rate of 100 mL min^{-1}) on a simultaneous SDT 2960 thermal analyzer from room temperature up to 700 ºC, with a heating rate of 10 ºC min^{-1}. The morphology of the as-prepared samples and the corresponding

energy dispersive X-ray (EDX) spectroscopy were obtained by using a Hitachi S-4800 field-emission scanning electron microscope (FE-SEM). The adsorption isotherm of nitrogen was measured at 77 K by using V-Sorb 2800P adsorption equipment. ESI-MS measurements were performed with an LCQ fleet mass spectrometer.

The electrochemical measurements were carried out by an electrochemical analyzer system, CHI660E (Chenhua Instrument, Shanghai, China) in a three-compartment cell with a platinum wire counter electrode, an Hg/HgO reference electrode and a working electrode. The electrolyte was a 6.0 M KOH aqueous solution and electrochemical impedance spectroscopy (EIS) measurements of as-synthesized samples were conducted at open circuit voltage in the frequency range of 100 kHz to 10 mHz.

3. Results and discussion

Three Schiff-base ligands, namely **L_1**, **L_2** and **L_3**, were designed as structure-building motifs since with the appropriate coordinating functionalities (CO_2H and nitrogen atom), the flexible shapes should give rise to unique coordination polymers with transition metal ion nodes. In a typical synthesis, the Schiff-base linkers were separately dissolved in *N,N*-dimethylformamide (DMF) to form a clear solution under heating, and the resulting solution was mixed with $Ni(OAc)_2$ aqueous solution and reacted for another 1h. During this time, formation of CPPs was observed (Scheme 1). The solid samples, tagged as CPP-1, CPP-2 and CPP-3 corresponding to separate linkers, were collected from the reaction mixture by centrifugation and washed with ethanol through several successive centrifugation and

re-dispersion cycles.

The morphology for the isolated CPPs was firstly characterized by field-emission scanning electron microscopy (FE-SEM) as illustrated in Fig. 1. The image of CPP-1 shows sheet-like architecture that has many holes and pores on it (Fig. 1a). The size for the holes range in 30–100 nm and the mean size of pores is around 11 nm (Fig. 1b). Altering the organic building blocks, the particle-like CPP-2 was obtained massively (Fig. 1c). Each particle ranged side by side with a mean size of 48 nm as shown in Fig. 1d. For this observation, it reveals that different organic linkers can construct distinct architectures because various coordination surroundings can be created through diverse coordination atoms. In comparison with the CPP-2, CPP-3 also displayed particle-like motif, but the morphology was not uniform. And there was no obvious single particle, each particle gathered together to form a cluster due to the high surface energy. This result illustrates that varying the position of coordination atom for allotrope can generate different morphologies due to the different coordination mode of ligand $\mathbf{L_2}$ and $\mathbf{L_3}$. We believe that more ordered CPPs will be generated by designing novel organic building blocks and adjusting the synthetic procedure in the future.

Then the structures of all the coordination polymer species CPP-1–CPP-3 were supported by X-ray powder diffraction (XRD) results as shown in Fig. 2a-c. The results suggest that CPP-1 is amorphous and CPP-2 and CPP-3 are both crystalline. However, the structure of CPP-2 and CPP-3 cannot correspond to any known phase of Ni-based metal-organic frameworks (based on the search results from CCDC [22]).

Although the use of single crystal X-ray diffraction methods, in many cases, is precluded to characterize the CPPs, they can be conveniently characterized by traditional methods, such as elemental analysis (EA), thermo-gravimetrical analyses (TGA) and infrared spectroscopy (IR). As can be clearly seen in Scheme 1, the chosen linkers possess different numbers of N atoms. After formation of CPPs, the CPP-1 should have much more N amount than that of CPP-2 and CPP-3, which is in good keeping with the EA results. The N amount is 12.96, 10.99 and 8.17% for CPP-1, CPP-2 and CPP-3, respectively, according to their EA results. The N amount for CPP-2 is larger than that of CPP-3 may suggest that DMF molecules are involved in the formation of CPPs, that is, the DMF molecules are participant in coordination or in lattice place. It can be confirmed by TGA results, as shown in Fig. 2d, which revealed two different decomposition curves. CPP-2 and CPP-3 were both stable up to 400 ºC, however, the solvent liberation for CPP-2 happened in the 50–200 ºC temperature range and CPP-3 occurred before 150 ºC, showing that CPP-2 possess more DMF molecules in inner structure and needs higher temperature to decompose. As compared, the initial weight loss for CPP-1 occurred before 100 ºC and could be ascribed to water liberation.

The formation of coordination polymers from metal ions and carboxylate-functionalized organic building blocks is well known in transition-metal coordination chemistry, and they can be easily detected by IR spectroscopy [23]. The infrared spectra of CPPs shows similar intense peak around 3350 cm^{-1} belonging to the O–H stretching band of the carboxylate group and/or the coordinated water

molecules. The characteristic bands of the carboxylate group for as-synthesized CPPs are shown at 1500–1610 cm^{-1} for anti-symmetric stretching and at 1372–1415 cm^{-1} for symmetric stretching. The absence of the expected bands at 1685–1715 cm^{-1} for the protonated carboxylate groups illustrates the complete de-protonation after the formation of CPPs (for details see Experimental section).

Taking advantage of the outstanding reactivity and thermal behaviors of CPPs, nickel oxides were then prepared by thermal treatment of CPP-1–CPP-3 at 450 ℃ in air. The decomposed products were first characterized by XRD spectra as listed in Fig. 3a. The entire observed peaks in all annealing samples match exactly with the standard values reported for NiO, which is a cubic phase (JCPDS No. 47-1049). The crystal structure for characteristic peaks of {111}, {200} and {220} crystal plane are depicted in Fig. 3b-c and Fig. S4. The Ni atom is surrounded by six oxygen atoms and form a 1D zigzag chain seen from {111} plane, and a network architecture viewing along {200} and {220} facet. It suggests that Ni atom re-coordinate with oxygen atom of air to form structural stable compounds (NiO) from Ni-based complex precursors in decomposing process. The chemical composition of the resulting products was further determined using EDX spectroscopy (Fig. S5). The EDX patterns confirm the presence of Ni and O in decomposition samples and the atom ration is close to 1:1, which is in accordance with the XRD results. The NiO products are denoted as porous NiO, NiO nanospheres and NiO nanoparticles corresponding to CPP-1–CPP-3 for avoiding misunderstanding, respectively.

The nominated names came out of the characterization of SEM as shown in Fig. 4.

Fig. 4a and 4b showed formation of a porous motif which evolved from CPP-1 precursor. The pores changed into more uniform due to the gas releasing of precursor in annealing process. As to NiO nanospheres (Fig. 4c and 4d), it inherited the morphology of CPP-2 and turn into more round with better dispersion. The diameter of a single sphere was *ca*. 30 nm. In comparison with the template, the size reduction suggests that the decomposing process has a vital influence on the sizes and shapes for resulting samples. Similar to NiO nanospheres, the NiO nanoparticles inherited the mother's shape and got smaller sizes during the decomposition process. The particles also gathered together to form a cluster-like motif like precursor CPP-3. These observations illustrate Ni-Schiff-base compounds, as templates or precursors, can be well transformed into NiO nanostructures with a wide range of shapes by adjusting the heating rate and temperature. The chemical transformation from Metal-Schiff base CPPs may provide a new methodology for generating functional metal oxides architectures.

To verify the applicability of as-synthesized NiO nanostructures as pseudo-capacitor electrodes, their electrochemical properties are investigated in terms of their cycling performance. Cyclic voltammetry (CV) and chrono-potentiometry (CP) measurements are performed. CV is firstly studied using the classical three electrode method in 6.0 M KOH electrolyte to measure the capacitances of NiO electrodes (shown in Fig. 5a-5c). The CV curves show two pairs of redox peaks, which come from the redox processes of NiO/NiOOH, are characteristics of the electrochemical pseudo-capacitors from reversible faradaic redox reactions occurring

within the electro-active materials. Obviously, the values that are obtained for the NiO structures directly depended on the scan rate as shown in Fig. 5d. The specific capacitance is determined to be 145, 153 and 45 F g^{-1} at a scan rate of 5 mV s^{-1}, suggesting the NiO nanospheres has the largest specific capacitance and the value of porous NiO is close to NiO nanospheres electrode (Fig. S6). Besides, the specific capacitance of NiO nanospheres is also much higher than that of porous NiO and nanoparticles at scan rates of between 5 and 200 mV s^{-1}. Since this proton transfer process is slow, higher scan rate leads to either depletion or saturation of the protons in the electrolyte inside the electrode during the redox process. Conversely, with lower scan rates, higher fractions of OH^- will have more favourable conditions to reach the electro-active NiO sites, and thus leading to higher available capacitance.

The intrinsic reason for the distinct performance could be attributed to the effect of morphology at first, especially the surface area in various architectures, which usually affects the charge transfer and ion diffusion rate of the NiO nanostructures, and therefore influencing the final electrochemical properties of electrodes. Brunauer-Emmett-Teller (BET) gas-sorption measurements of the NiO electrodes confirmed this point as shown in Fig. 6a-c. Based on the gas-sorption results, the BET specific surface area for porous motif, nanospheres and nanoparticles is 50.6, 48.0 and 35.5 m^2 g^{-1}, respectively. The result shows that the higher surface area the samples are, the larger the specific capacitance will be, since the specific capacitance is based on faradic charge-transfer reactions with the OH^- ions and is dependent on its accessibility to the electro-sites of NiO active materials. Secondly, the Nyquist plots

of all NiO samples are presented to further explain the various performances as listed in Fig. 6d. The electrochemical impedance spectroscopy (EIS) data can be fitted by an equivalent circuit, which consists of a bulk solution resistance (R_s), a charge-transfer resistance (R_{ct}), a constant phase element (CPE) to account for the double layer capacitance, and a pseudocapacitive element (C_p) from the redox process of NiO, as depicted in Fig. S7. The R_s value of three electrode samples is calculated (measured with ZsimpWin software) to be 0.77, 0.67 and 0.56 Ω, respectively, while the corresponding R_{ct} values were calculated to be 2.9, 1.8 and 22.3 Ω (porous NiO, nanospheres and nanoparticles separately correspond to black, red and blue line). It is noticed that the NiO nanospheres exhibit smaller electrochemical reaction impedance, indicating that nanospheres have smaller charge transfer resistance and weaker polarization and therefore displaying better performance.

Galvanostatic charge-discharge curves at different constant current densities, within the potential range 0–0.5 V vs. Hg/HgO of the three NiO electrodes are illustrated in Fig. 7a-c. NiO nanospheres show a much lower charge voltage plateau and higher discharge voltage platform than porous NiO and NiO nanoparticles counterparts, which is consistent with CV measurements. Moreover, the increase in charging time represents the higher capacitance and the calculated specific capacitance at current density of 0.2 A g^{-1} is 92, 89 and 55 F g^{-1}, respectively, demonstrating the positively morphology and resistance influence (Fig. S8). The specific capacitances for three NiO electrodes at different current densities are calculated and the corresponding relationships are shown in Fig. 7d. The specific

capacitance increases for lower charge-discharge rates because of the diffusion-controlled redox reaction between the OH^- ions and the NiO samples. Although there are some reports showing much higher specific capacitances for NiO [24-26], we believe that taking into consideration of the morphology and resistance effect in the research work, more NiO electrodes with lower resistance, higher surface area and better electrochemical performance will be prepared in the future.

Because it is important for an electro-capacitor material to have good cycling performance, an endurance test is employed using CV measurement to examine the cycle life for the above-mentioned NiO electrodes (Fig. 8a-d). The specific capacitance for porous NiO electrode grows larger during the first 50 cycles [24,25] and then decreased slightly over the rest of 950 cycles. The appeared summit might be due to an electrochemical activation process of electrode that electrolytes in general require a period of time to penetrate the entirely interior space of an active electrode material. After 1000 continuous cycles, the capacitance retention is 99% (Fig. 8a, 8c). For NiO nanospheres electrode, the capacity peak maintained in the first 150 cycles and then decreased over the next 850 cycles with the capacitance retention is 100% (Fig. 8b, 8d). This cycling result indicates that NiO nanospheres exhibits better cycling performance than the other two electrodes, which is also in contrast with other reported NiO electrodes [26-32].

4. Conclusion

In conclusion, cubic phase NiO electrodes with distinct morphologies have been fabricated by chemical transformation of nanoscale Ni-Schiff-base coordination

polymer precursors. The porous NiO and NiO nanospheres exhibit better electrochemical properties with weaker polarization, better reversibility and enhanced capacitance (145 and 153 F g^{-1} at 5 mV s^{-1}) and cycling performance (close to 100% capacitance retention) than NiO nanoparticles, indicating higher surface area and smaller charge-transfer resistance the samples are, the larger the specific capacitance will be. In this regard, more NiO electrodes will be synthesized using the "Schiff-base-type" precursors and serve as promising candidates in energy storage fields.

Acknowledgements

This work was supported by the Fundamental Research Funds for the Central Universities (KYZ201540) and the Scientific Research Foundation of Nanijng Agricultural University (050804087).

References

[1] M. Oh, C.A. Mirkin, Nature 438 (2005) 651.

[2] P. Horcajada, T. Chalati, C. Serre, B. Gillet, C. Sebrie, T. Baati, J.F. Eubank, D. Heurtaux, P. Clayette, C. Kreuz, J.-S. Chang, Y.K. Hwang, V. Marsaud, P.-N. Bories, L. Cynober, S. Gil, G. Férey, P. Couvreur, R. Gref, Nat. Mater. 9 (2010) 172.

[3] A.M. Spokoyny, D. Kim, A. Sumrein, C.A. Mirkin, Chem. Soc. Rev. 38 (2009) 1218.

[4] M. Oh and C. A. Mirkin, Angew. Chem., Int. Ed. 45 (2006) 5492.

[5] J.D. Rocca, D.M. Liu, W.B. Lin, Acc. Chem. Res. 44 (2011) 957.

[6] A. Carné, C. Carbonell, I. Imaz, D. Maspoch, Chem. Soc. Rev. 40 (2011) 291.

[7] J.H. Lee, S. Kang, J.Y. Lee, J.H. Jung, Soft Mater. 8 (2012) 6557.

[8] W.J. Rieter, K.M.L. Taylor, H. An, W. Lin, W. Lin, J. Am. Chem. Soc. 128 (2006) 9024.

[9] T. Tsuruoka, S. Furukawa, Y. Takashima, K. Yoshida, S. Isoda, S. Kitagawa, Angew. Chem. Int. Ed. 48 (2009) 4739.

[10] K. Liu, H.P. You, Y.H. Zheng, G. Jia, L.H. Zhang, Y.J. Huang, M. Yang, Y.H. Song, H.J. Zhang, CrystEngComm 11 (2009) 2622.

[11] Z. Ni, R.I. Masel, J. Am. Chem. Soc. 128 (2006) 12394.

[12] Y.-M. Jeon, G.S. Armatas, D. Kim, M.G. Kanatzidis, C.A. Mirkin, Small 5 (2009) 46.

[13] I. Imaz, M. Rubio-Martínez, L. García-Fernández, F. García, D. Ruiz-Molina, J. Hernando, V. Puntes, D. Maspoch, Chem. Commum. 46 (2010) 4737.

[14] S. Jung, M. Oh, Angew. Chem. Int. Ed. 47 (2008) 2049.

[15] K.B. Wang, Y.X. Yin, C.Y. Li, Z.R. Geng, Z.L. Wang, CrystEngComm 13 (2011) 6231.

[16] I. Imaz, M. Rubio-Martínez, W.J. Saletra, D.B. Amabilino, D. Maspoch, J. Am. Chem. Soc. 131 (2009) 18222.

[17] C. Jo, H.J. Lee, M. Oh, Adv. Mater. 23 (2011) 1716.

[18] L. Zhang, X. Qian, L. Liu, Z. Shi, Y. Li, S. Wang, H. Liu, Y. Li, Chem. Commun. 48 (2012) 6166.

[19] W. Cho, Y.H. Lee, H.J. Lee, M. Oh, Adv. Mater. 23 (2011) 1720.

[20] K. Wang, X. Ma, Z. Zhang, M. Zheng, Z. Geng, Z. Wang, Chem. Eur. J. 19 (2013) 7084.

[21] K.B. Wang, X.B. Shi, A.M. Lu, X.Y. Ma, Z.Y. Zhang, Y.N. Lu, H.J. Wang, Dalton. Trans. 44 (2015) 151.

[22] The Cambridge Structural Database: a quarter of a million crystal structures and rising. F. H. Allen, Acta Cryst., B58 (2002) 380.

[23] O. M. Yaghi, M. O•Keeffe, N.W. Ockwig, H.K. Chae, M. Eddaoudi, J. Kim, Nature 423 (2003) 705.

[24] Y.F. Yuan, X.H. Xia, J.B. Wu, X.H. Huang, Y.B. Pei, J.L. Yang, S.Y. Guo, Electrochem. Commun. 13 (2011) 1123.

[25] W. Du, R. Liu, Y. Jiang, Q. Lu, Y. Zhang, F. Gao, J. Power Sources 227 (2013) 101.

[26] A. Paravannoor, R. Ranjusha, A. M. Asha, R. Vani, S. Kalluri, K.R.V. Subramanian, N. Sivakumar, T.N. Kim, S.V. Nair, A. Balakrishnan, Chem. Eng. J. 220 (2013) 360.

[27] Z.H. Gao, H. Zhang, G.P. Cao, M.F. Han, Y.S. Yang, Electrochim. Acta 87 (2013) 375.

[28] B. Ren, M. Fan, Q. Liu, J. Wang, D. Song, X. Bai, Electrochim. Acta 92 (2013) 197.

[29] A. Allagui, A. H. Alami, E.A. Baranova, R. Wüthrich, J. Power Sources 262 (2014) 178.

[30] H. Pang, Q.Y. Lu, Y.C. Li, F. Gao, Chem. Commun. 48 (2009) 7542.

[31] M.B. Zheng, Z.X. Ling, S.T. Liao, Z.J. Yang, G.B. Ji, J.M.Cao, J. Tao, Acta Chim. Sinica 67 (2009) 1069.

[32] X.H. Xia, J.P. Tu, X.L. Wang, C.D. Gu, X.B. Zhao, J. Mater. Chem. 21 (2010) 671.

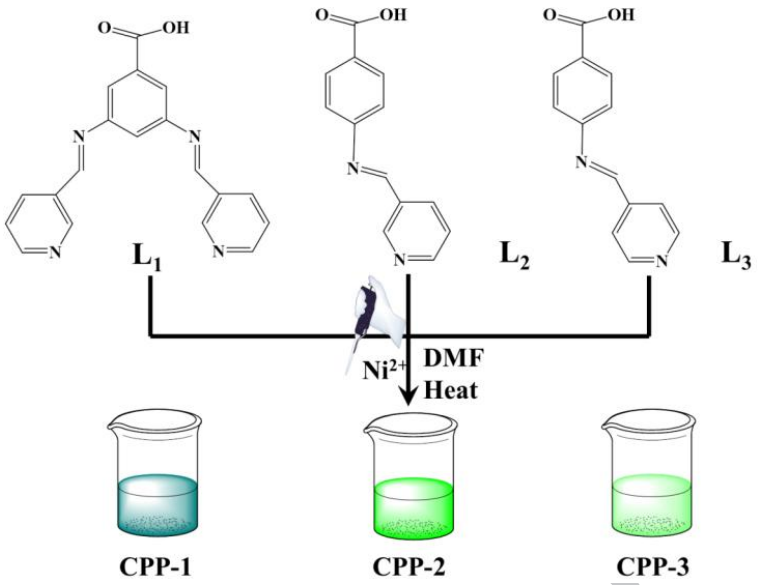

Scheme 1.

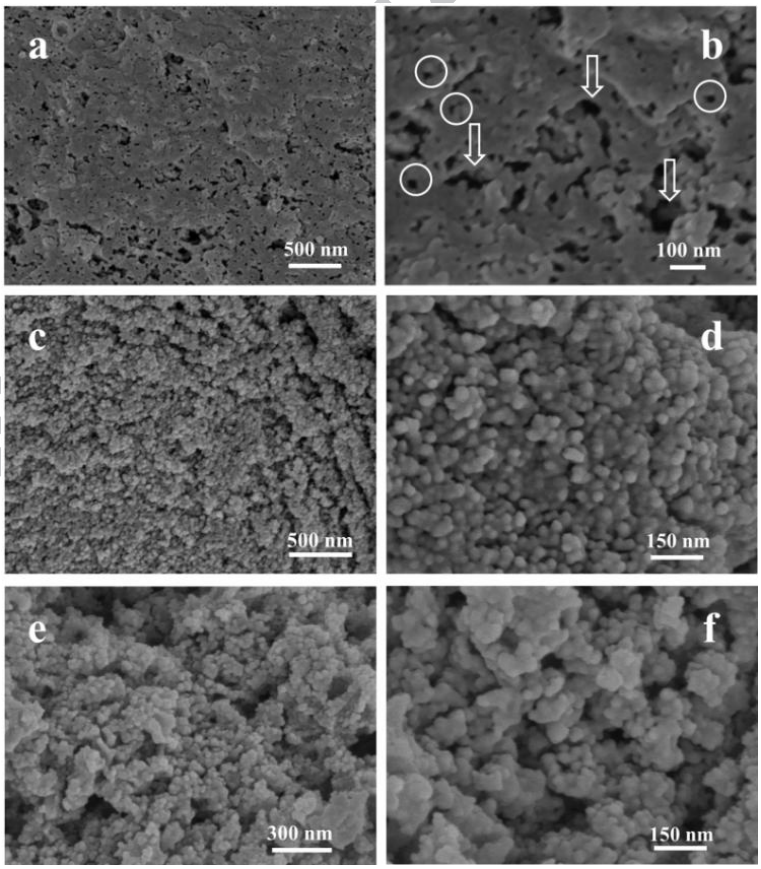

Fig. 1.

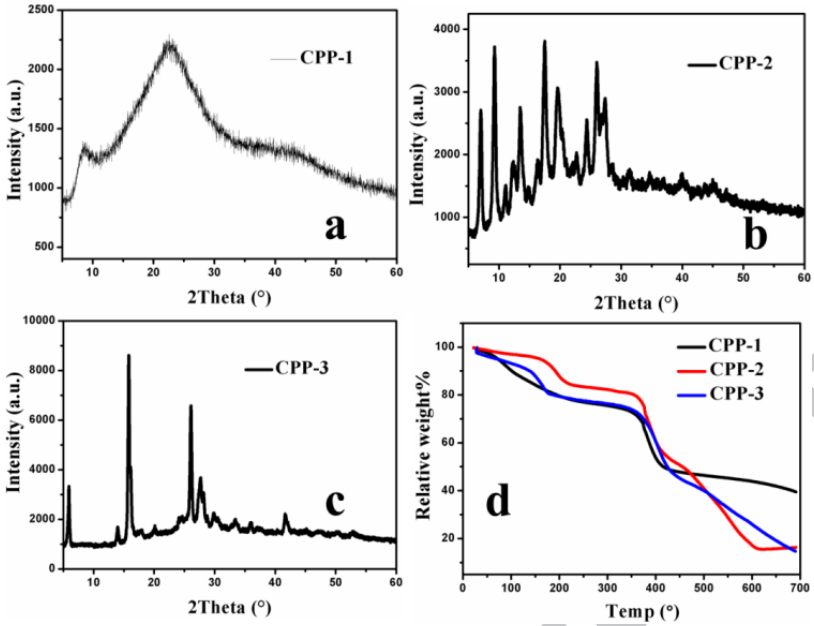
CPP-1
Intensity (a.u.)
2Theta (°)
a
CPP-2
Intensity (a.u.)
2Theta (°)
b
CPP-3
Intensity (a.u.)
2Theta (°)
c
CPP-1
CPP-2
CPP-3
Relative weight%
Temp (°)
d

Fig. 2.

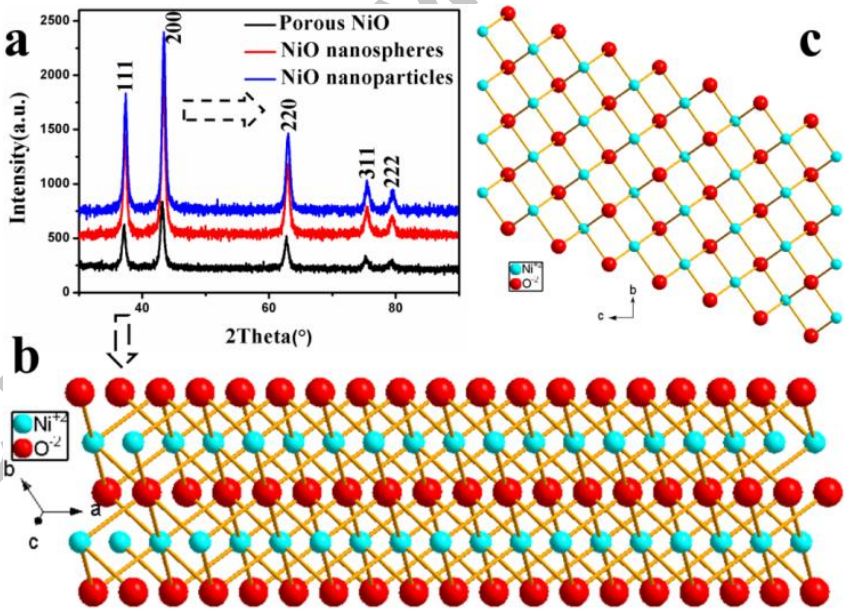
a
Porous NiO
NiO nanospheres
NiO nanoparticles
Intensity(a.u.)
2Theta(°)
111
200
220
311
222
c
b
Ni+2
O-2
a
b
c

Fig. 3.

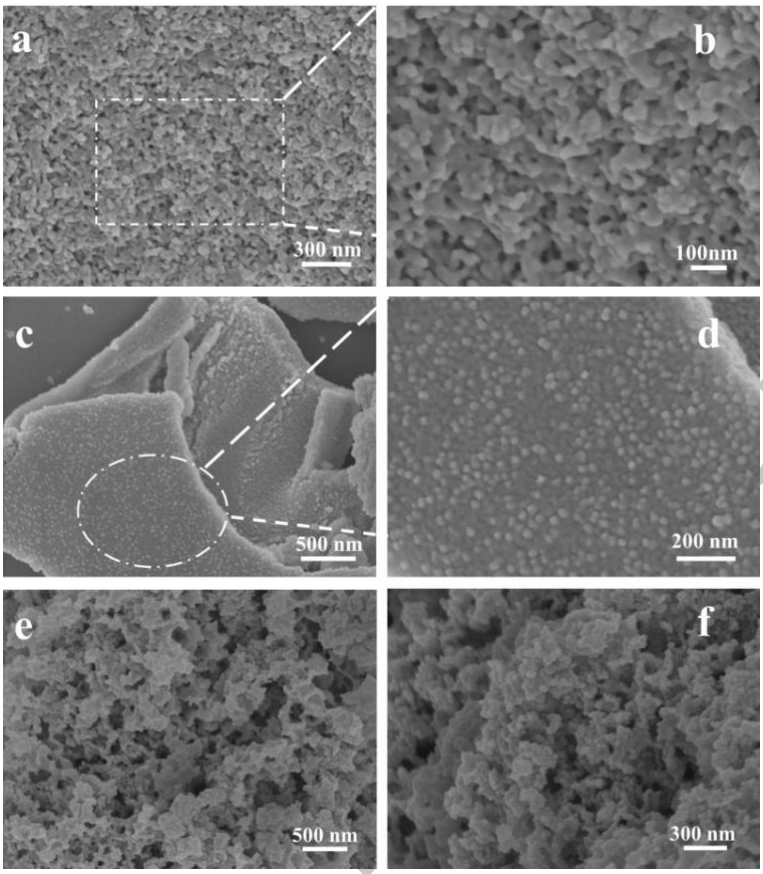

Fig. 4.

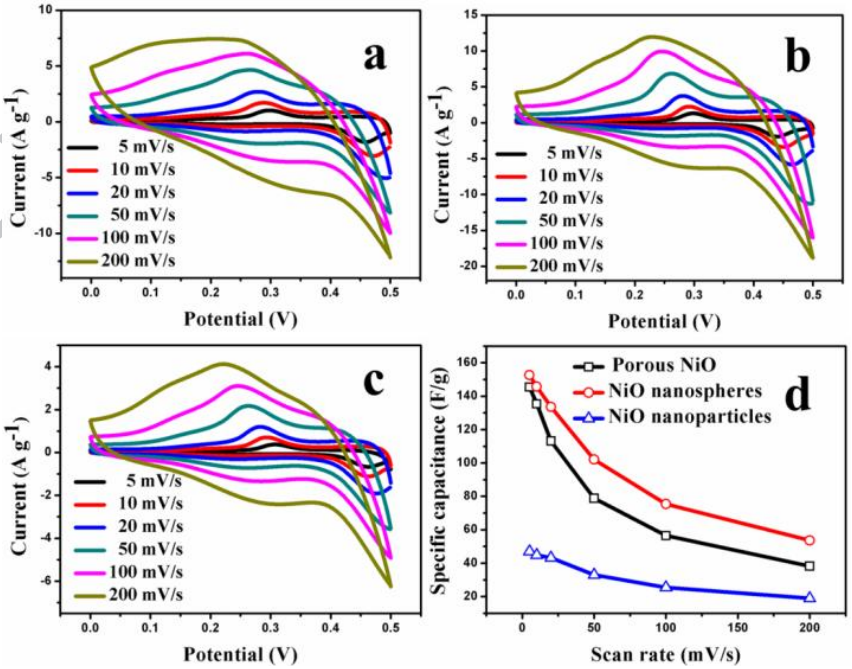

Fig. 5.

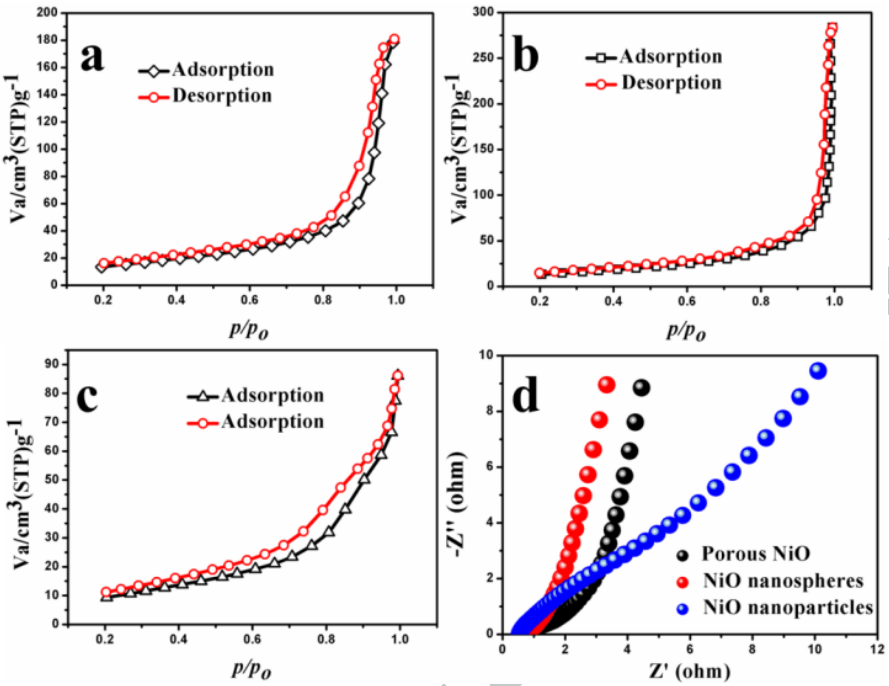

Fig. 6.

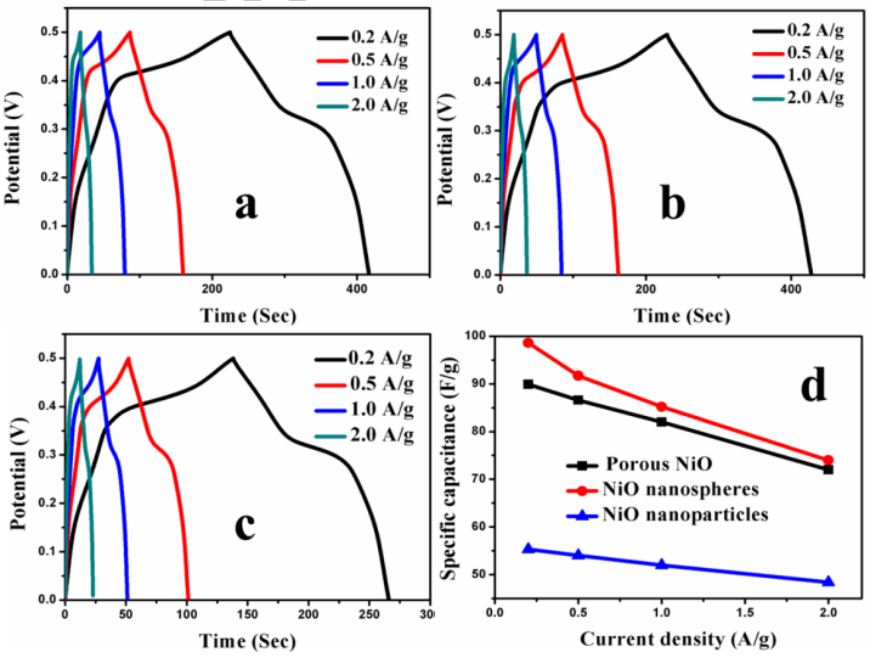

Fig. 7.

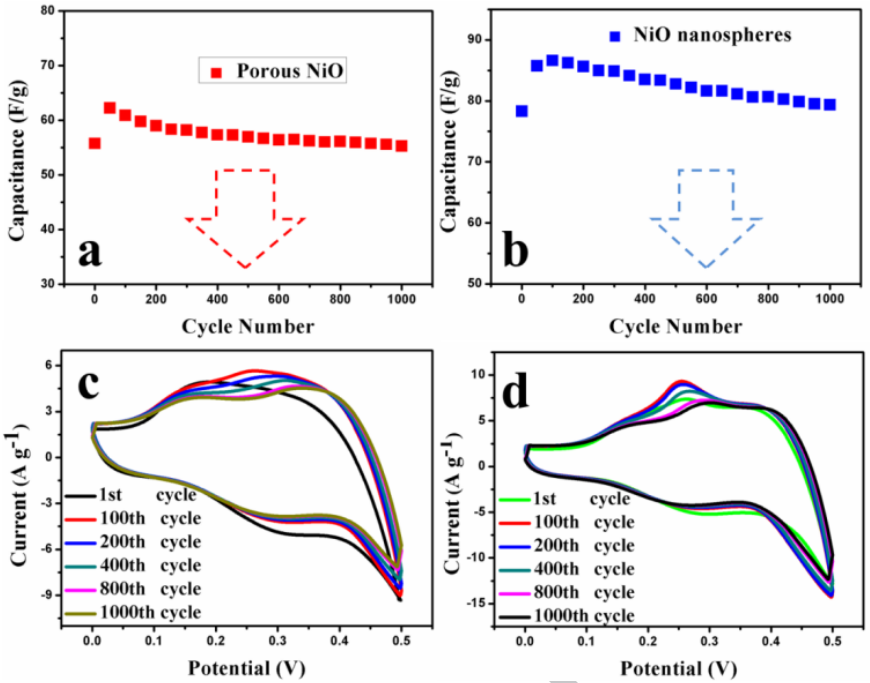

Fig. 8.

Graphic Abstract-Pictogram

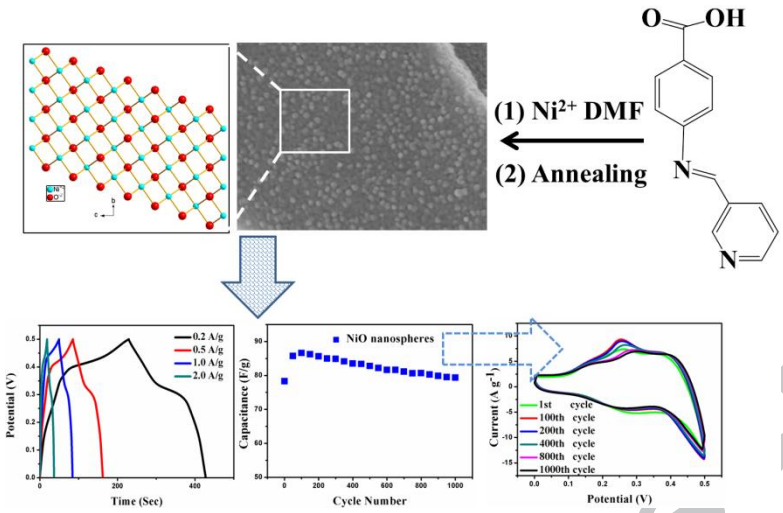

Graphic Abstract-Synopsis

NiO nanostructures have been synthesized from Schiff-base building blocks. Among them, NiO nanospheres show higher capacitance than the other two electrodes with 100% retained capacitance after 1000 cycles at a constant scan rate.